



AMS
American Meteorological Society

Supplemental Material

[© Copyright 2020 American Meteorological Society](#)

Permission to use figures, tables, and brief excerpts from this work in scientific and educational works is hereby granted provided that the source is acknowledged. Any use of material in this work that is determined to be “fair use” under Section 107 of the U.S. Copyright Act or that satisfies the conditions specified in Section 108 of the U.S. Copyright Act (17 USC §108) does not require the AMS’s permission. Republication, systematic reproduction, posting in electronic form, such as on a website or in a searchable database, or other uses of this material, except as exempted by the above statement, requires written permission or a license from the AMS. All AMS journals and monograph publications are registered with the Copyright Clearance Center (<http://www.copyright.com>). Questions about permission to use materials for which AMS holds the copyright can also be directed to permissions@ametsoc.org. Additional details are provided in the AMS Copyright Policy statement, available on the AMS website (<http://www.ametsoc.org/CopyrightInformation>).

Supplementary Material for “An Integrated Geometric and Topological Approach for Identification and Visual Analysis of Rossby Wave Packets”

KARRAN PANDEY

Department of Computer Science and Automation, Indian Institute of Science, Bangalore

JOY MERWIN MONTEIRO

Department of Earth and Climate Science, Indian Institute of Science Education and Research, Pune

VIJAY NATARAJAN

Department of Computer Science and Automation, Indian Institute of Science, Bangalore

ABSTRACT

This document presents additional material supporting the paper “An Integrated Geometric and Topological Approach for Identification and Visual Analysis of Rossby Wave Packets”. It includes graph plots and figures describing additional results from the sensitivity analysis. A few figures provide background information and present results of additional experiments for one of the case studies from the paper.

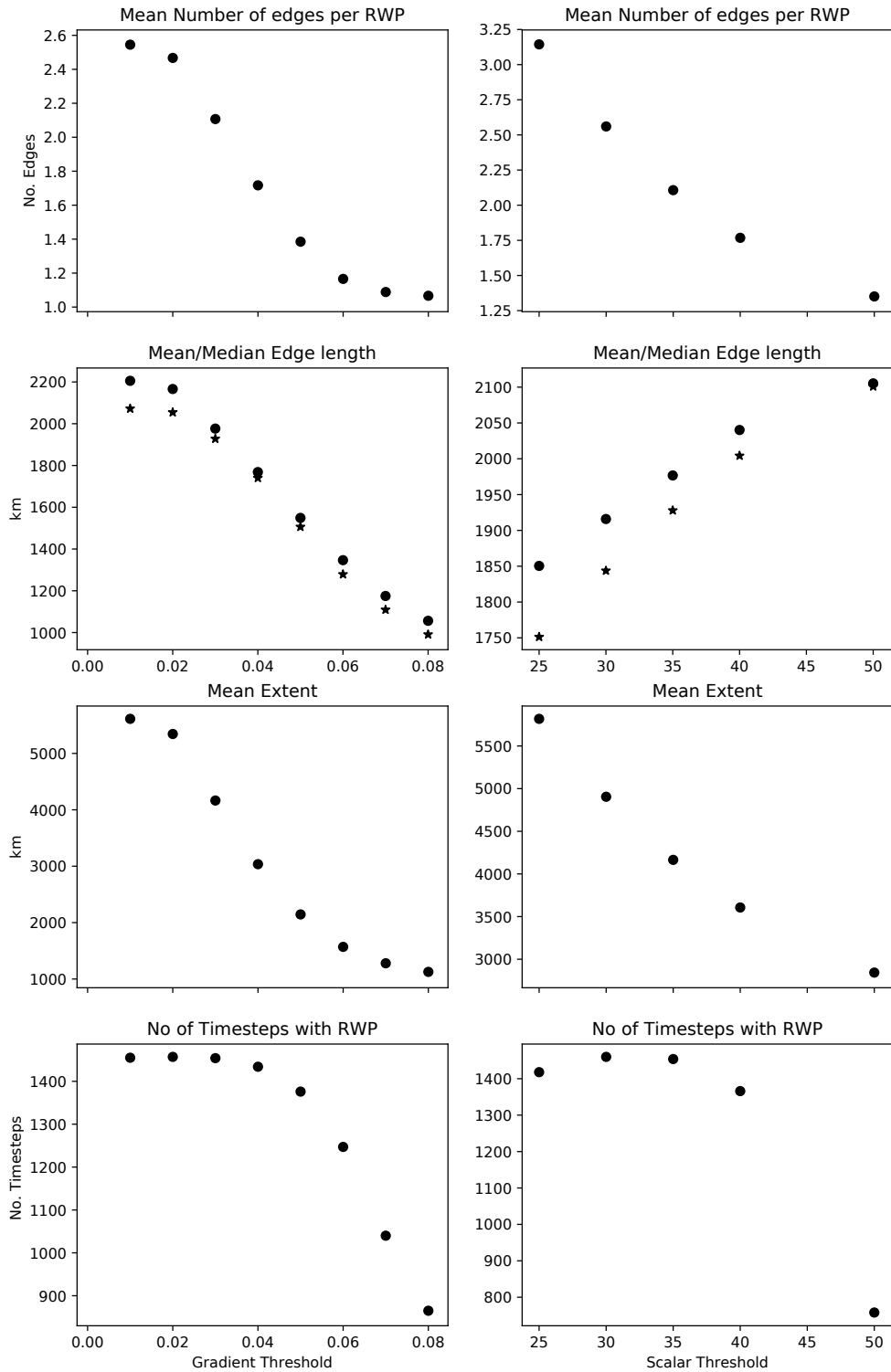


FIG. 1. The spatial statistics of the identified RWPs in spring (March-May) when (left) the gradient weight threshold GT is varied and (right) the scalar weight threshold ST is varied. The edge length is calculated as the haversine distance between the end point nodes. The mean extent of the RWP is calculated by adding the lengths of all edges in the pruned association graph. The total number of time steps in the data is 1440.

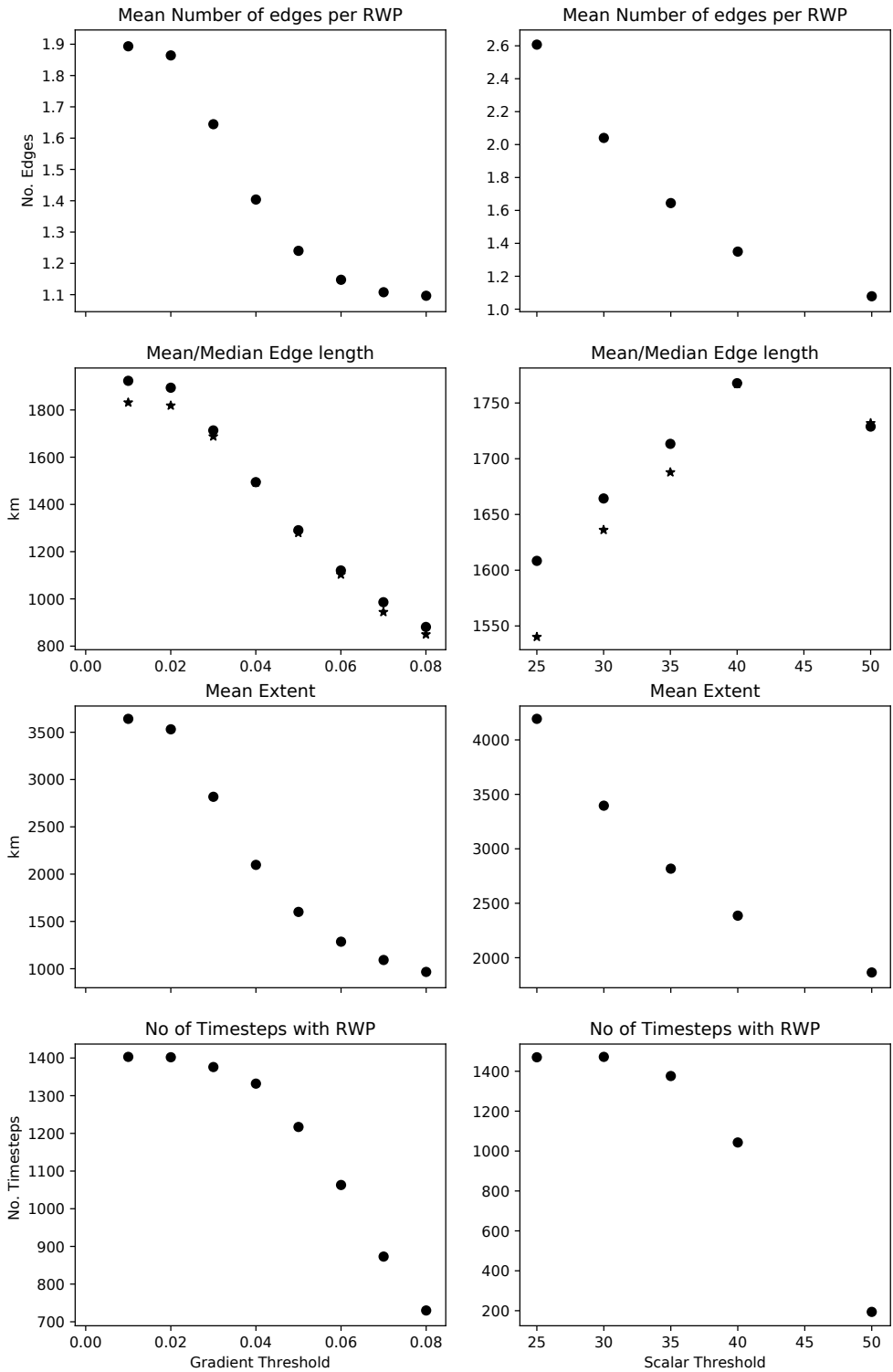


FIG. 2. The spatial statistics of the identified RWPs in summer (June-August) when (left) the gradient weight threshold GT is varied and (right) the scalar weight threshold ST is varied. The edge length is calculated as the haversine distance between the end point nodes. The mean extent of the RWP is calculated by adding the lengths of all edges in the pruned association graph. The total number of time steps in the data is 1440.

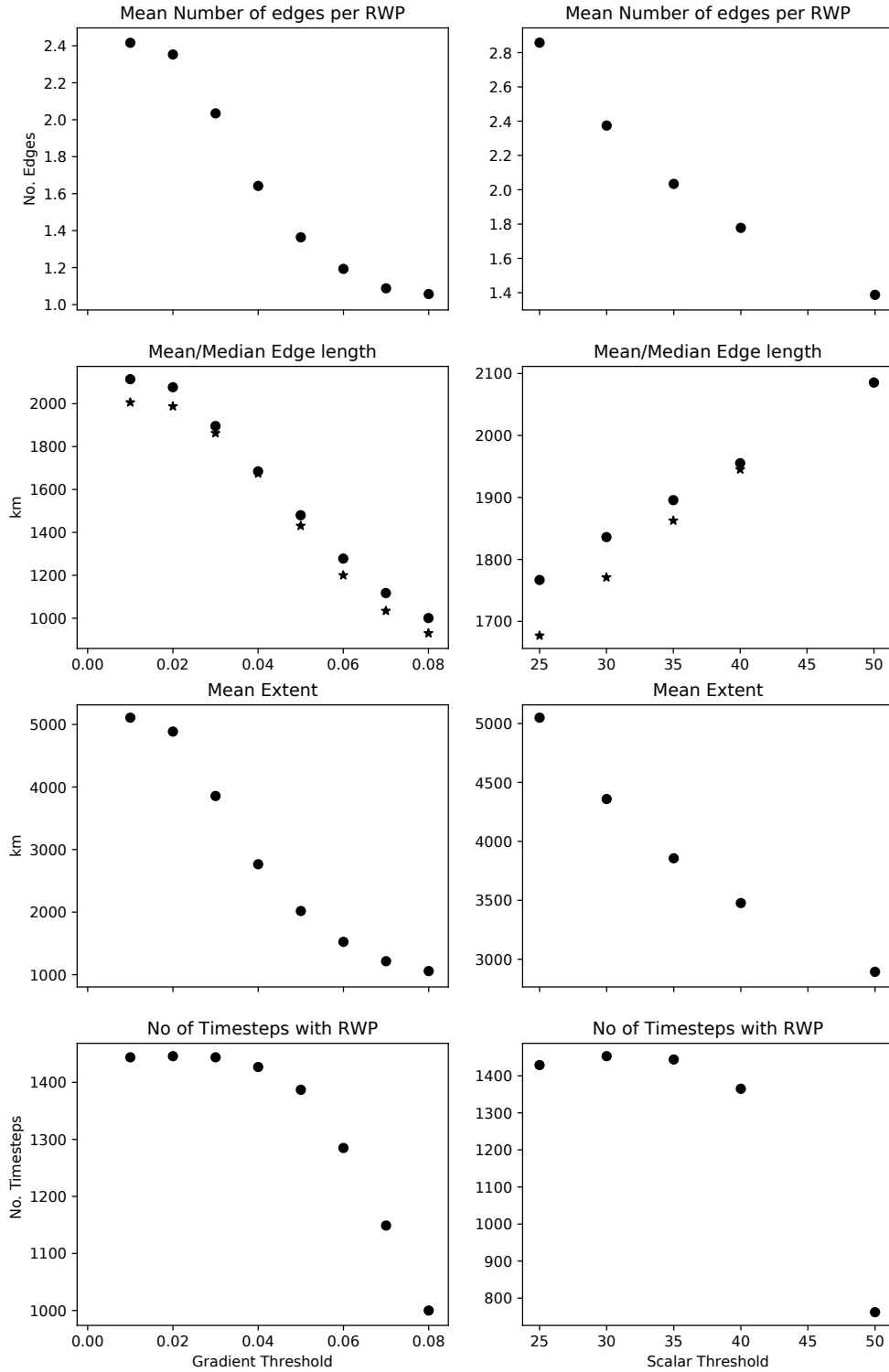


FIG. 3. The spatial statistics of the identified RWPs in fall (September-November) when (left) the gradient weight threshold GT is varied and (right) the scalar weight threshold ST is varied. The edge length is calculated as the haversine distance between the end point nodes. The mean extent of the RWP is calculated by adding the lengths of all edges in the pruned association graph. The total number of time steps in the data is 1440.

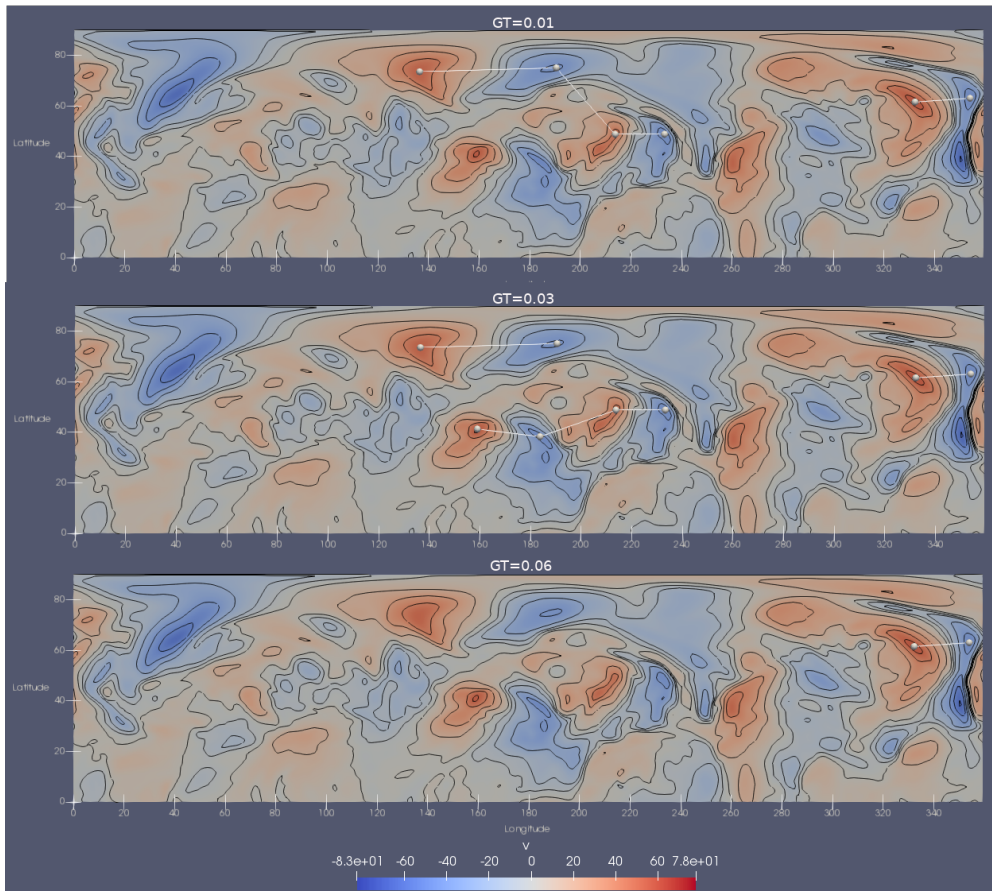


FIG. 4. The sensitivity of the identified RWP paths to variations in the gradient edge threshold (GT). A scalar threshold of 35 m/s is used. The northern hemispheric meridional winds (300 hPa) on 1800 UTC, January 3, 1990 is used for comparison. The white dots and connecting lines represents the identified RWP paths. For a low value of GT (top), the algorithm tends to connect RWPs that are visually well-separated. For moderate values of GT (middle), the algorithm produces RWP paths that match our intuition of the different RWPs in the field. A high value of GT (bottom) only captures intense dipole structures.

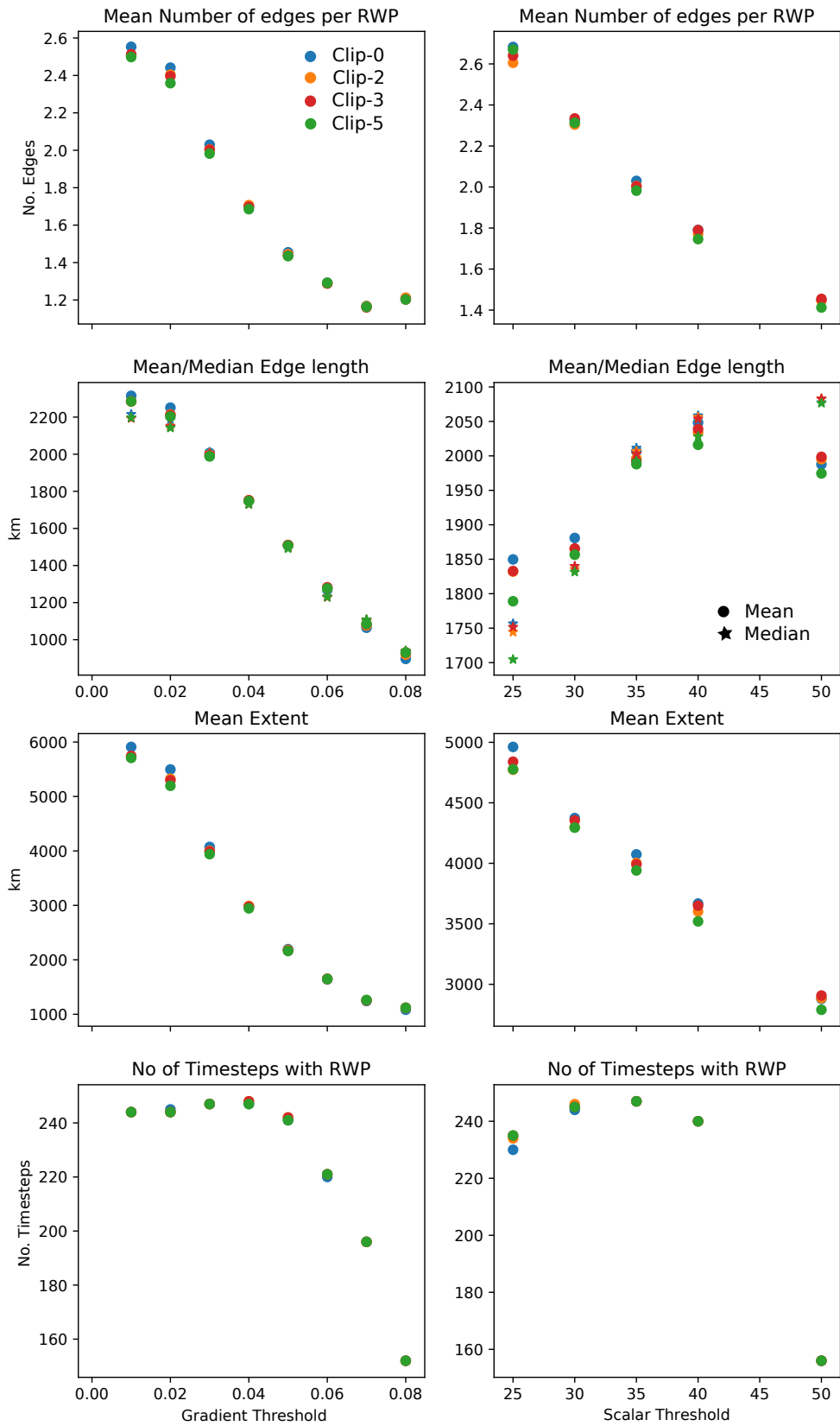


FIG. 5. The sensitivity of the RWP statistics to variations of the clip value. Blue, Orange, Red and Green refer to clip values of 0, 2, 3, 5 respectively.

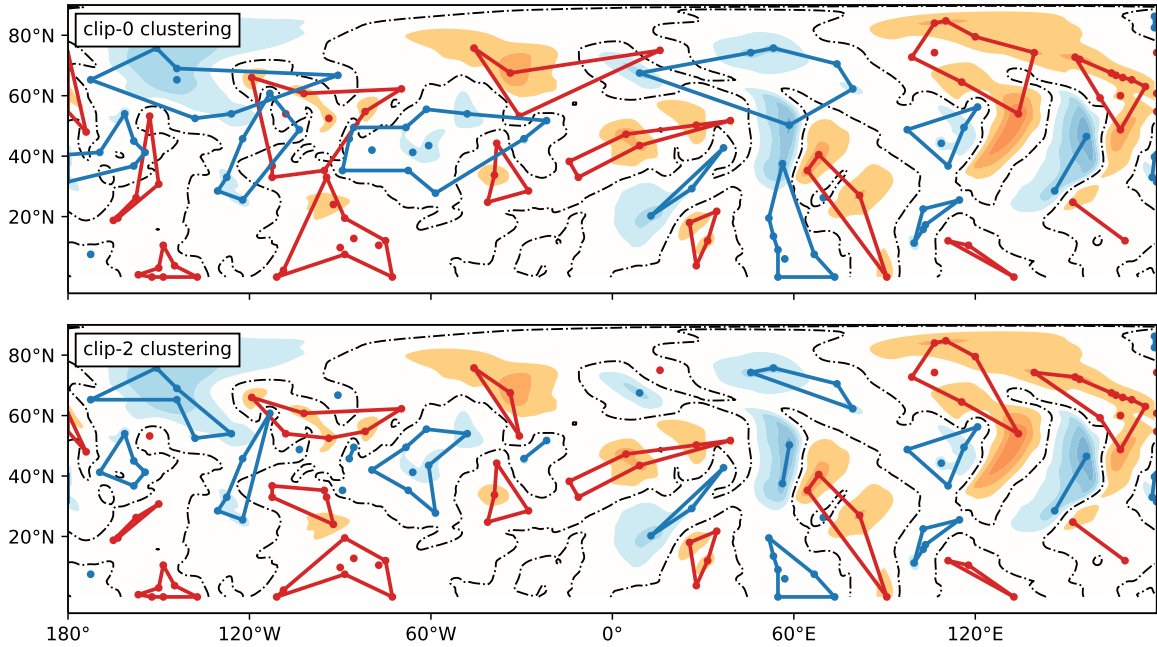


FIG. 6. The identified clusters using the 0 m/s isocontour (top) and 2 m/s isocontour (bottom) for the northern hemispheric meridional winds (300 hPa) on 1200 UTC, January 2, 1990. A scalar threshold of 35 m/s and gradient threshold of 0.03 are used. The blue (red) dots represent the identified local minima (maxima). The blue (red) polygons are formed by connecting all boundary minima (maxima) that belong to a single cluster. The boundary minima (maxima) are denoted by blue (red) dots. Note that some minima/maxima lie within the polygon since the polygon represents the boundary of the cluster. The 0 m/s isocontour is marked using a dashed-dotted line. Clustering using the 0 m/s isocontour tends to cluster together weak maxima/minima into a larger cluster. This is clearly visible for the weak minima clusters between 180W-5W, 20-80N. Using the 2 m/s isocontour largely eliminates this issue. Higher amplitude clusters are largely retained as is, as seen in the clusters between 60-180E.

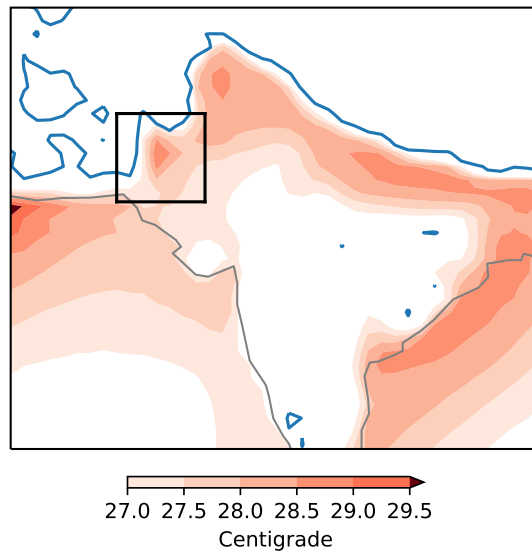


FIG. 7. The distribution of wet-bulb temperatures in South Asia. The contours represent the 99th percentile of the wet-bulb temperatures in the region. The blue line represents the 800 meter elevation isocontour. The region of interest is bounded by a black box. This figure is adapted from Fig. 1 in (Monteiro and Caballero 2019)

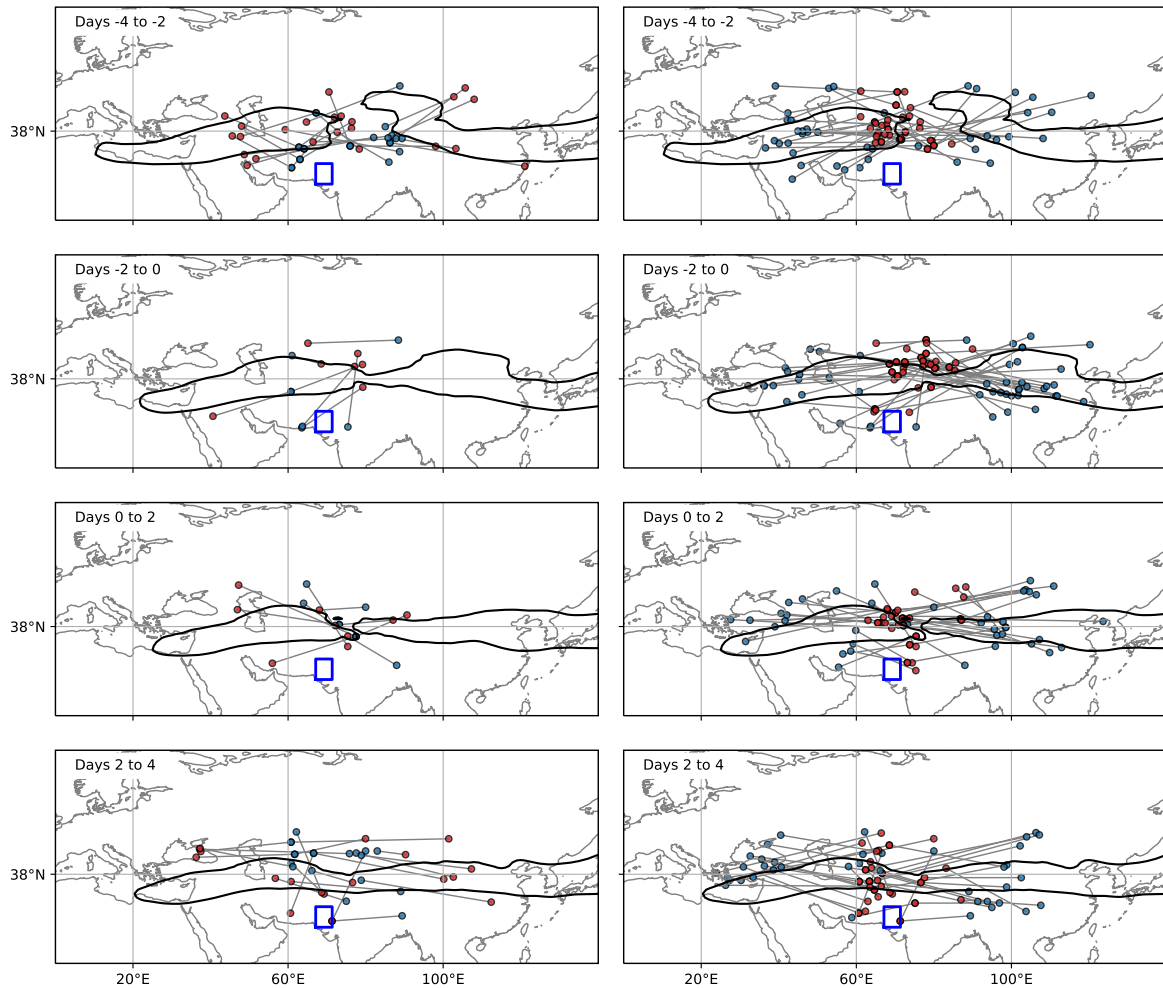


FIG. 8. The RWP structure during events where the meridional winds associated with the RWP is southerly over the region of interest (60-90°E). The left (right) column shows those RWPs that have a v -min cluster (v -max cluster) between the longitudes 60-90°E. Blue dots represent minima or flow from the north and red dots represent maxima or flow from the south. The 20 m/s contour of the zonal winds associated with the events is plotted for reference. Each panel contains all RWPs in the two day period indicated in the label. We note that even though we have selected for events with predominantly southerly winds, there are a small number of northerly wind events (in the panel to the left) which are associated with meridionally oriented RWPs which have both a v -max cluster and v -min cluster in the region of interest.

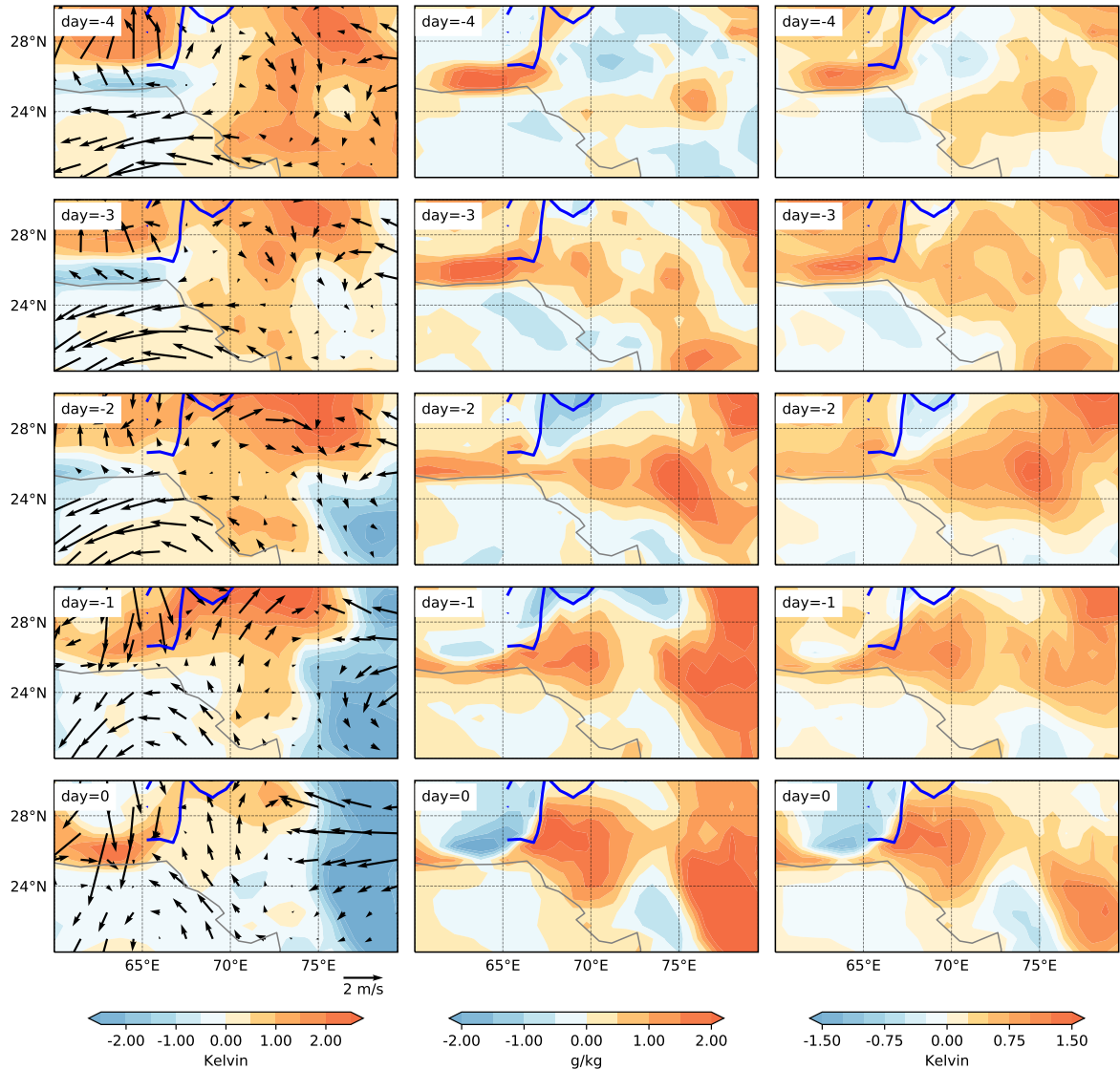


FIG. 9. The composite evolution of the surface fields during the events when the RWP associated meridional wind are southerly over 60-90°. The left column shows anomalies of temperature and winds. The center column shows anomalies of specific humidity and the right column shows anomalies of wet-bulb temperature.

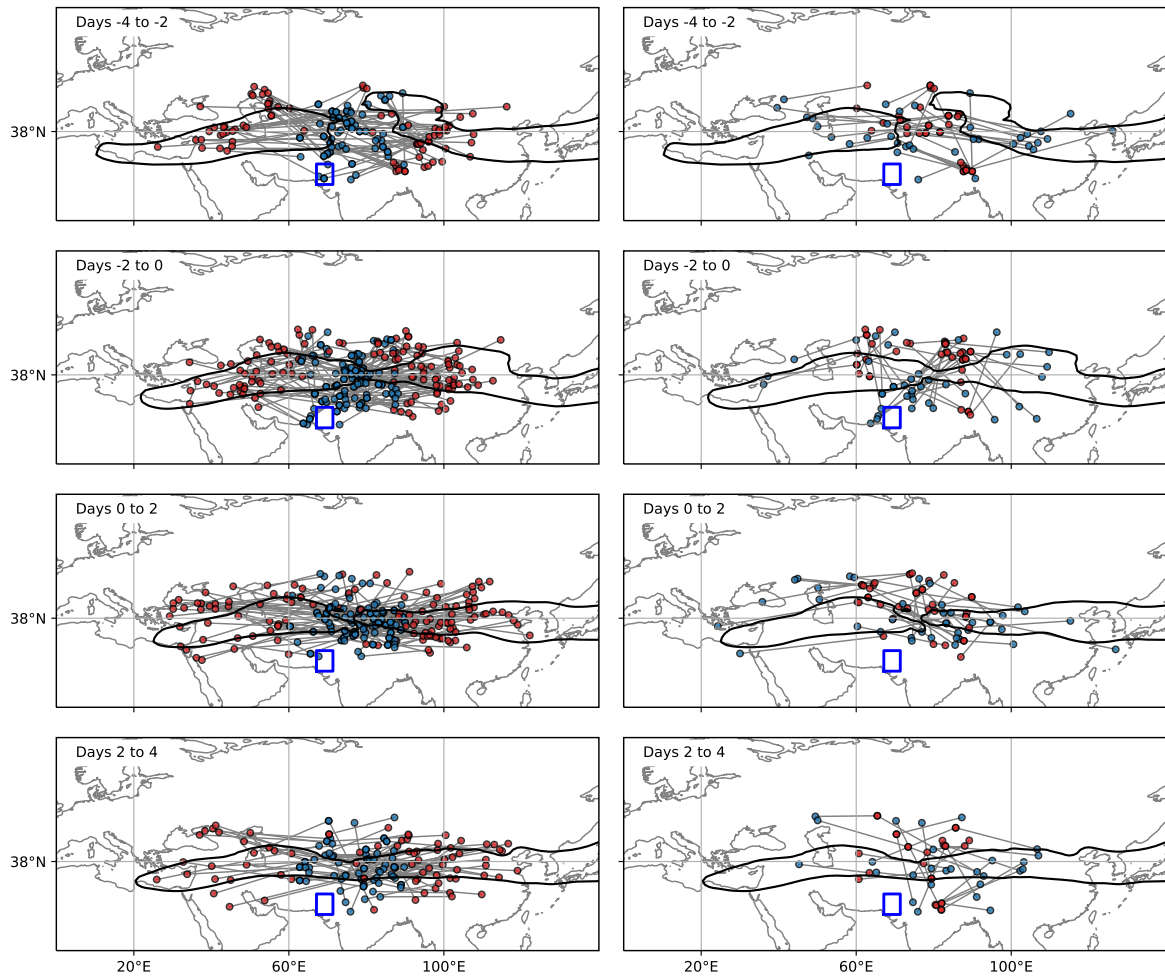


FIG. 10. The RWP structure during events where the meridional winds associated with the RWP is northerly over the region of interest (60–90°E). The left (right) column shows those RWPs that have a v -min cluster (v -max cluster) between the longitudes 60–90°E. Blue dots represent minima or flow from the north and red dots represent maxima or flow from the south. The 20 m/s contour of the zonal winds associated with the events is plotted for reference. Each panel contains all RWPs in the two day period indicated in the label. We note that even though we have selected for events with predominantly northerly winds, there are a small number of southerly wind events (in the panel to the left) which are associated with meridionally oriented RWPs which have both a v -max cluster and v -min cluster in the region of interest.

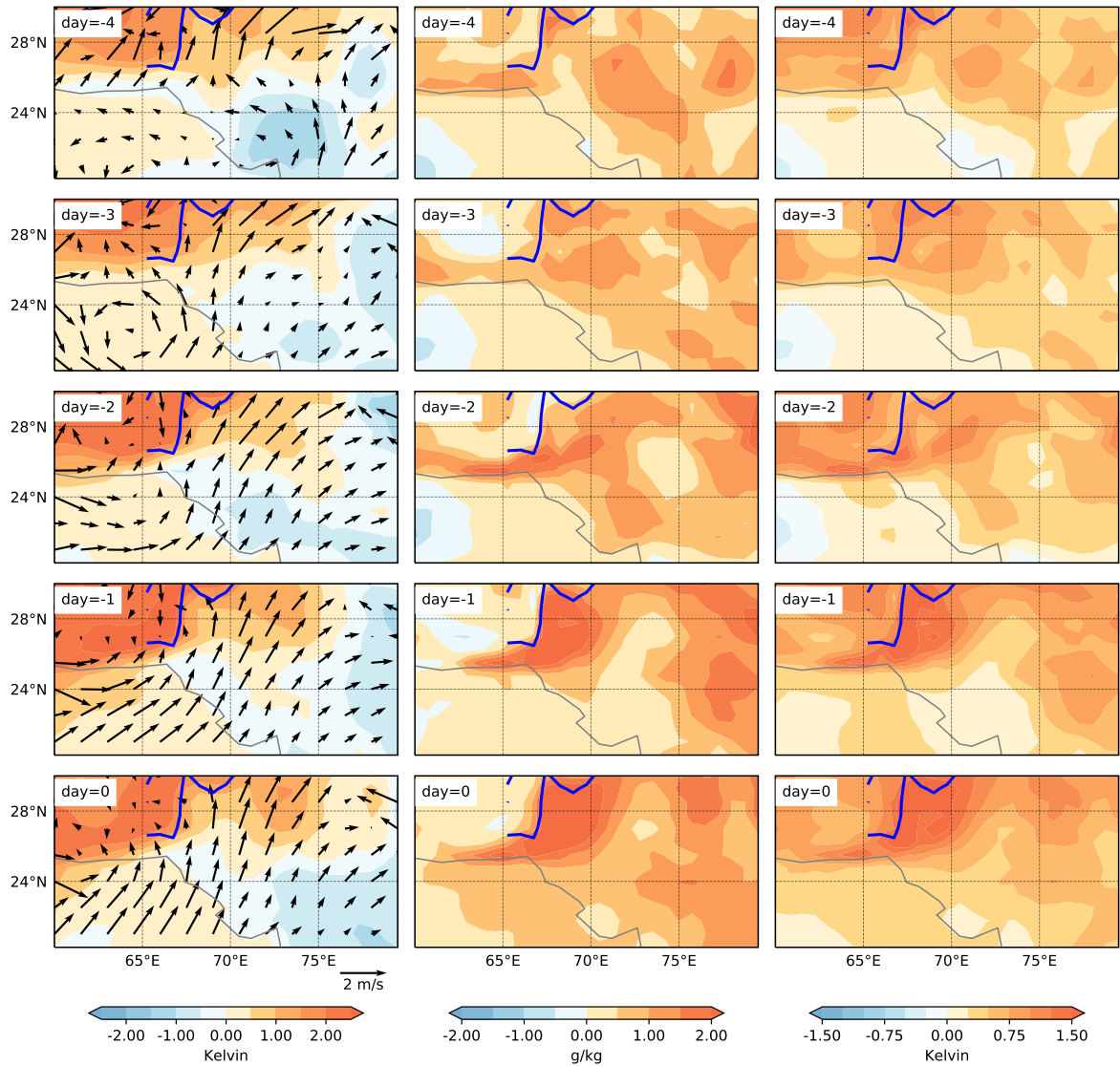


FIG. 11. The composite evolution of the surface fields during the events when the RWP associated meridional wind are northerly over 60-90°. The left column shows anomalies of temperature and winds. The center column shows anomalies of specific humidity and the right column shows anomalies of wet-bulb temperature.

References

Monteiro, J. M., and R. Caballero, 2019: Characterization of extreme wet-bulb temperature events in southern pakistan. *Geophysical Research Letters*, **46** (17-18), 10 659–10 668, doi:10.1029/2019GL084711, URL <https://agupubs.onlinelibrary.wiley.com/doi/abs/10.1029/2019GL084711>, <https://agupubs.onlinelibrary.wiley.com/doi/pdf/10.1029/2019GL084711>.